Civil Engineering Dimension
https://ced.petra.ac.id

Axial Compression Capacity of Finger-Jointed Laminated Board Made from Rubber Wood Species

Awaludin, A.[1]*, Shulhan, M.A.[2], Effendi, M.K.[3], and Hassan, R.[4]
[1] Department of Civil and Environmental Engineering, Universitas Gadjah Mada, Yogyakarta, INDONESIA
[2] Department of Civil Engineering, Universitas Sarjanawiyata Tamansiswa, Yogyakarta, INDONESIA
[3] Department of Civil Engineering, Universitas Janabadra, Yogyakarta, INDONESIA
[4] Institute for Infrastructure Engineering and Sustainable Management (IIESM), Universiti Teknologi MARA, Shah Alam, MALAYSIA

DOI: https://doi.org/10.9744/ced.27.2.113-122

Article Info:
Submitted: Apr 24, 2025
Reviewed: June 17, 2025
Accepted: July 18, 2025

Keywords:
finger-jointed laminated board,
rubberwood species,
axial compression capacity,
affordable housing,
buckling failure.

Corresponding Author:
Awaludin, A.
Department of Civil and Environmental Engineering, Universitas Gadjah Mada, Yogyakarta, INDONESIA
Email: ali.awaludin@ugm.ac.id

Abstract

The utilisation of Rubberwood was an effort to provide an alternative to low-cost housing in Indonesia. This study investigated the use of Rubberwood Finger-Jointed Laminated Board (FJLB) under compression loading parallel to the grain. The investigation included laboratory experiments and numerical analysis. The experiments were conducted using two specimens of FJLB members, each with a length of 2000 mm and a cross-sectional dimension of 100 mm × 100 mm². Finite element analysis (FEA) was employed to predict the axial capacity, considering non-linearity, contact boundary conditions, and buckling analysis of the material. The study found an average axial capacity of 150.9 kN for the two specimens, which was 3.2% higher than the FEA and 5.4% higher compared to the Euler formula. Laboratory measurements revealed that initially, the stress distribution in the cross-section was uniform, then suddenly changed to a combination of tension and compression during the final loading stage.

This is an open access article under the CC BY license.

INTRODUCTION

Housing construction in Indonesia is expected to increase suddenly in the coming years. According to Statistics Indonesia, only 60.9 % of Indonesian households have access to suitable housing, leaving a shortage of approximately 26.9 million housing units as of 2022, which will continue to rise [1]. Moreover, the population of the country is projected to double by 2045 compared to 2015 levels [2]. Jakarta Property Institute [3] reported that the housing backlog in 2045 is expected to increase by 3.5 times unless the government implements a major intervention program. To tackle this problem, Indonesian government planned a one million-house program through Ministry of Public Works and Housing in 2015 [4,5]. Despite the success of the program in 2021, an annual backlog is still expected since the program can only reduce the gap by approximately 4% each year [4]. Therefore, a breakthrough in finance, construction technology, and government regulation should be conducted to overcome this problem.

The government and industry have developed several types of prefabricated houses that are affordable and quicker to build than conventional masonry homes recently in Indonesia. The prefabricated houses are mainly categorized by the main structural material including cold-formed steel, hollow square-section hot-rolled steel, pre-cast concrete, and timber. In the last five years, these types of dwellings have been used in post-disaster reconstruction projects throughout the country [6–8]. Based on Lombok earthquake post-disaster program, a prefabricated house made from engineered wood products, namely Cross Laminated Timber (CLT) was the most efficient variant. This variant has

Note : Discussion is expected before November, 1st 2025, and will be published in the "Civil Engineering Dimension", volume 28, number 1, March 2026.
ISSN : 1410-9530 print / 1979-570X online
Published by : **Petra Christian University**

a sufficient floor area, the lowest cost of construction, good seismic resistance, and the material is categorized as sustainable [8,9].

Future development of prefabricated houses in Indonesia will primarily focus on engineered wood products, such as Finger-Jointed Laminated Board (FJLB) made from Rubberwood species (*Hevea brasiliensis*). The main advantages of the wood species are the high strength-to-weight ratio, custom-sizing, and high resistance to termite attack or aggressive environments [10–12]. Additionally, FJLB is made from small Rubber wood lamina with a dimension of 20 by 20 by 400 mm, which is glued and pressed to assemble the desired structural element size (Figure 1). The finger joints connect each lamina in the longitudinal direction to improve the glue bond by increasing the contact area (Figure 1b) [12]. As a raw material, the Rubber tree is famous as a natural latex source, which is spread over 3.4 million hectares of Rubber plantations in Indonesia. After a 25-year productive period, the trees are cut down and used as the materials for FJLB products [12]. Moreover, the processing of wood from raw material to finished product leads to a lower CO_2 emission than other materials such as concrete and steel [13,14].

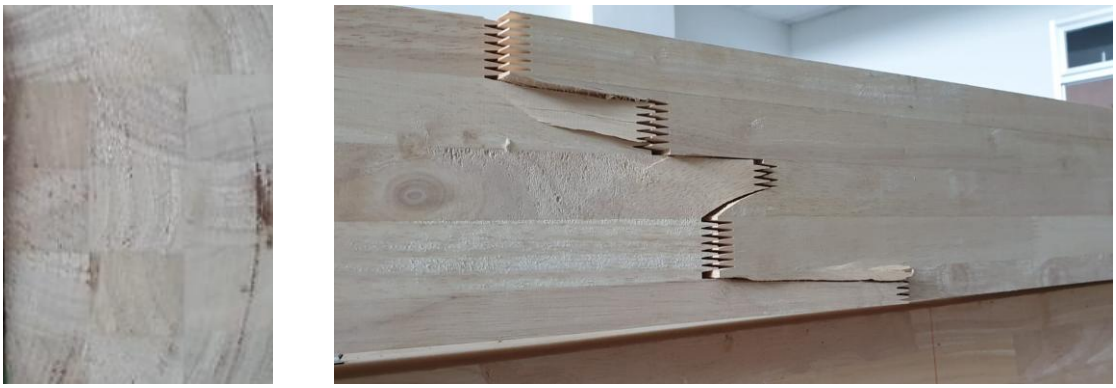

(a) (b)

Figure 1. (a) FJLB Beam Cross-section and (b) Finger Joint along the Longitudinal Axis

The use of FJLB is limited to non-structural building components. This investigation assesses the performance of FJLB under compression loading, recognizing the potential of the rubber wood product for structural use. As a compression member, FJLB is subjected to load in the longitudinal direction, which is vulnerable to buckling and fiber-crushing failure [15]. Previous studies by Li et al. [16] and Zhou et al. [17] discovered that crushing failure appeared in short columns while buckling occurred in longer columns. Buckling failure includes excessive lateral deflection, correlating with slenderness ratio [17]. The system reduces the axial capacity of a compression member because buckling failure (σ_{cr}) occurs below the final stress (σ_u) of the material [18]. The study of buckling resistance of bamboo columns has been provided by Nugroho et al. [15] and Bahtiar et al. [19]. This resistance (σ_{cr}) was determined experimentally by testing short, medium, and long bamboo column specimens. Buckling reduction factor (ψ) was determined using various regression methods based on the experimental data. Additionally, the regression of Ylinen provided a reliable reduction factor (ψ) for the bamboo column design parameter.

Finite element method has been applied to predict the buckling behavior of glulam-bamboo by Li et al. [16]. Following the discussion, two methods were included in ANSYS software, namely non-linear and eigenvalue buckling analysis. Li et al. [16] found that non-linear buckling analysis was more accurate because it accommodated the non-linearity and large-deflection response of the material. Moreover, the complexity of numerical analysis of buckling behavior increases because the wood has asymmetric strength properties in tension and compression, potentially leading to brittle as well as ductile failure simultaneously [10,20–23]. Previous studies proved the fracture mechanics method was suitable for modeling the brittle problem, while plasticity theory in combination with the criterion of Hill successfully modeled the ductile problems [12,20–24].

This study aimed to examine the axial capacity of FJLB compression members subjected to a concentric load using experimental and numerical methods. The axial compression test on two FJLB column specimens was conducted in the laboratory to verify the numerical computation on MSC Marc/Mentat software that considered anisotropy and non-linearity material properties [25]. This numerical modelling strategy provided satisfactory results in predicting both linear and non-linear behaviour of wood-based engineered materials [25]. Furthermore, a parametric study was conducted to estimate the axial capacity of another cross-section and the length of the compression member, while maintaining a constant column slenderness ratio to provide insight for practical usage.

METHODS

FJLB used in this study was a mass product available on the building markets produced by PT. Puncak Menara Hijau Mas. During the process, engineering properties of the material including density, modulus of elasticity (MoE), and modulus of rupture (MoR) were evaluated based on BS-373:1957 (*British Standard Methods of Testing Small Clear Specimens of Timber*). MoE and MoR were assessed by a three-point loading bending test with specimens having a cross-section of 20 mm by 20 mm with a length of 280 mm. In addition to shear strength test, tensile and compressive strengths were evaluated both parallel and perpendicular to the grain with the results shown in Table 1.

Table 1. Mechanical Properties of FJLB [8,12]

Properties	Symbol	Value
Modulus of elasticity in tension (MPa)	E_t	10026.20
Modulus of elasticity in compression (MPa)	E_c	2640.30
Modulus of elasticity in bending (MPa)	E_b	7742.72
Compressive strength parallel-to-the-grain (MPa)	σ_{c11}	44.18
Tension strength parallel-to-the-grain (MPa)	σ_{t11}	80.50
Compressive strength perpendicular-to-the-grain (MPa)	σ_{u22}	11.24
Tension strength perpendicular-to-the-grain (MPa)	σ_{u22}	4.23
Shear strength (MPa)	τ_{12}	9.43
Shear modulus (MPa)	G_t	1077.60
Poisson's ratio	ν_{12}	0.23
Poisson's ratio	ν_{21}	0.05
Density (gr/mm^3)	ρ	0.63

During the experimental study, two FJLB members with a length of 2000 mm and a cross-section of 100 mm by 100 mm were tested. In the set-up, the test pieces were mounted vertically, sitting on a steel plate support and a coupled of steel spheres to emulate joints, as shown in Figure 2. The position of the specimen was carefully connected to ensure its verticality and concentricity. Following the process, the axial load, generated by a 30 kN hydraulic actuator, was applied gradually to the specimen at a loading rate of about 0.825 kN/sec. A linear variable data transducer (LVDT), positioned 100 mm from the lower support, was used to measure the axial displacement of the specimen. In addition, axial strain at the mid-span and quarter-span of the specimen was measured using strain gauges, as shown in Figure 2.

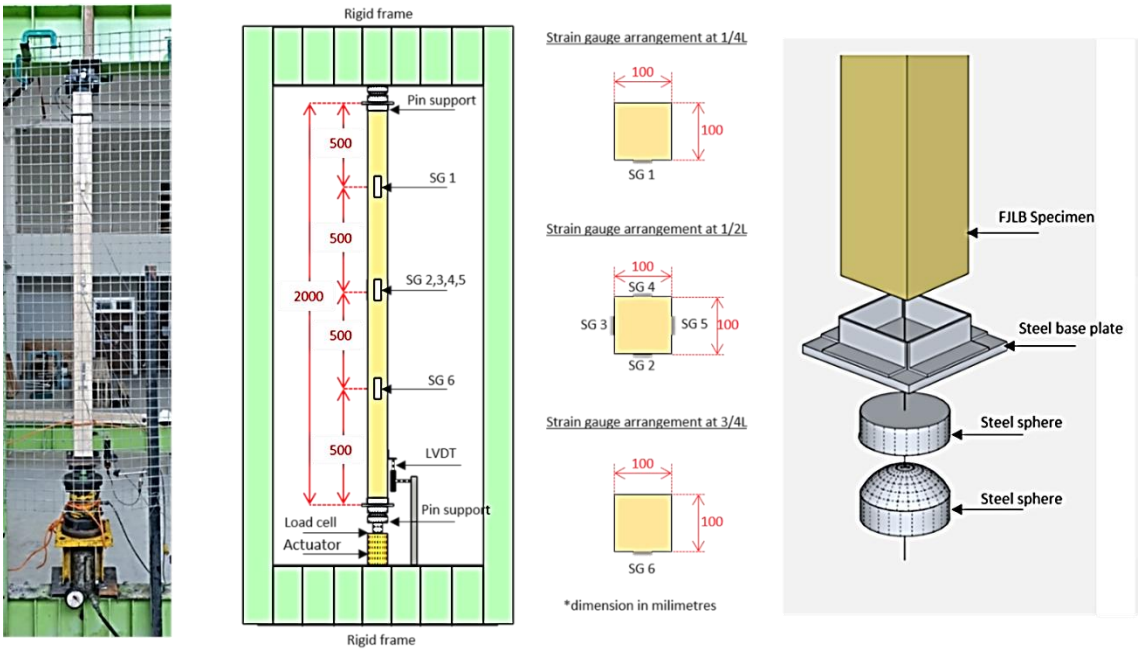

Figure 2. *Test* Setup for Pin-ended Column

FJLB specimen and its support were modeled three-dimensionally (3D) through MSC Marc/Mentat using hexahedron elements that featured eight nodes and three degrees of freedom per node for meshing. The mesh size of the material member was set to 17 x 17 x 17 mm^3 to produce a converged finite element result. Since FJLB consisted of six lamella layers, each lamella was modeled as a separate layer with glue contact type, signifying that all the elements

were perfectly connected. Following the process, the finger joint along the lamella was not included in finite element analysis (FEA) model since there was a limitation on the mechanical properties and computational resources of the joint. However, Shakimon et al. [26] and Serrano et al. [27] stated that the modeling strategy excluding the glue line and finger joint could still adequately predict the final load.

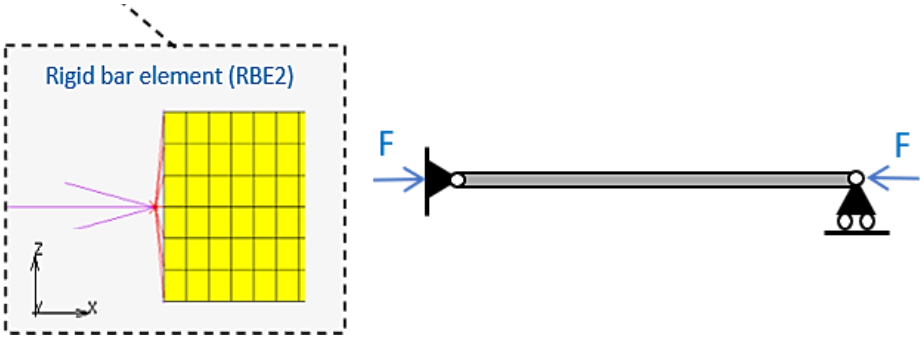

Figure 3. The 3D Model of FEA Study

As shown in Figure 3, the boundary conditions at both ends of the specimen were modeled using multi-point constraints with a rigid bar element (RBE2) to simulate the joint rotation and translation (column shortening). RBE2 created a web of rigid elements connected to an independent node. This process allowed the loads and nodal displacements to be transferred from many dependent nodes to an independent node. Moreover, the mechanical properties of FJLB (Table 1) were used to construct the constitutive model of FJLB. According to Awaludin et al. [24], the elastoplastic model with the identical modulus of elasticity (MoE) in both tension and compression was recommended.

In this FEA study, the yield criterion of Hill, with isotropic hardening rules, was adopted to account for the non-linearity of the wood material [28,29]. The Hills yield criterion was characterised by an ellipsoidal yield surface as illustrated in Figure 4 [30].

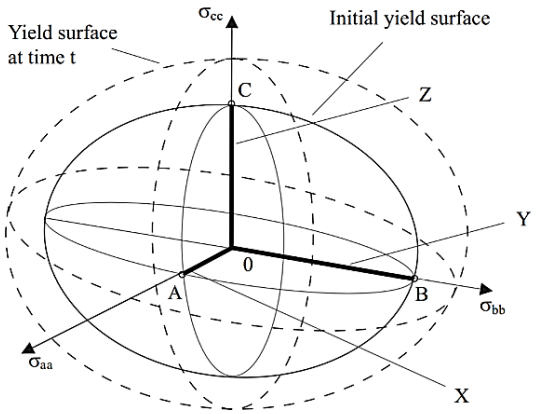

Figure 4. The Hills Yield Surface [30]

The results of FEA were evaluated and compared to the experimental results, allowing a better modeling strategy to be obtained. After FEA modeling was considered satisfactory and produced a good agreement with the experimental results, the model was further used in the parametric study of axial capacity under compression force for other cross-sections of members with the same slenderness ratio as the tested members. The dimension of these members was 125 mm x 125 mm x 2500 mm and 150 mm x 150 mm x 3000 mm.

RESULTS AND DISCUSSION

Figure 5 showed the final situation of specimen where FJLB member failed by buckling. This buckling was marked by excessive lateral deflection, which became more significant with the increased axial load. The failure of the specimens at the mid-span was identified as a tension fiber failure propagated from the finger joint location on the tension side (Figure 5). Moreover, finger joint failure of FJLB specimen was also found previously by Shulhan et al. [12], signifying that the joint was a weak point in the members. The buckling failure mode was often found in a

column specimen with a slenderness ratio greater than 12 (L/d > 12) or categorized as a long column specimen [15,16,29]. During the study, the response of FJLB compression member was subjected to concentric axial load as shown in Figure 6, signifying the relationship between axial load and axial displacement. Figure 6 showed that the axial displacement for FJLB1 specimen increased linearly until failure at 150.98 kN corresponding to 4.1 mm axial displacement. Consequently, the second test (FJLB2) showed a non-linear phase just before failure, reaching 153.45 kN with an axial displacement of 4.9 mm.

Figure 7 showed the relationship between axial stress and longitudinal strain of FJLB specimen. The axial stress data were obtained from axial load measurement divided by the area of cross-section, which was 100 cm^2. Meanwhile, longitudinal strain was obtained directly from strain gauge measurement, which was placed according to Figure 2. The stress-strain response at the quarter-span of FJLB members was then plotted in Figure 7(a), while Figure 7(b) showed the response at the mid-span of members.

Figure 5. The Buckling Failure of the Specimen

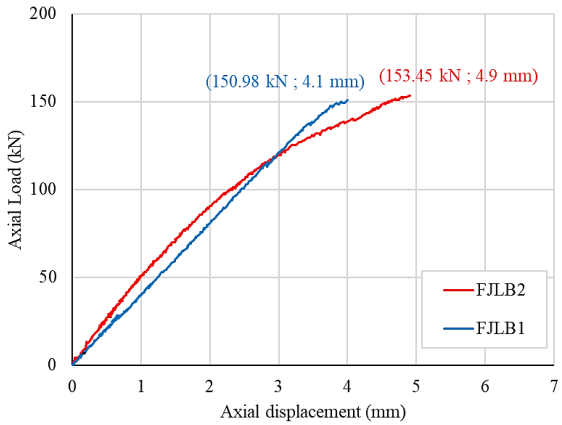

Figure 6. Experimental Load-axial Displacement Response

Figure 7(a) showed how strain at the quarter span of the specimen developed as the applied axial load increased. In the early stage of loading (axial stress less than 6 MPa), both strain gauge SG1 and SG6 had a negative strain, signifying that the member was in a compression state. After the axial stress reached 6 MPa, the stress-strain response gradually changed from linear to non-linear. Before reaching the final stress (15.09 MPa), the strain drastically reversed direction and increased until the specimen failed. Following this discussion, the strain measurement recorded that the SG1 failed at the strain of -0.0005 while the SG6 failed at the strain of 0.0007. The strain value showed that

both strain gauges (SG1 and SG6) experienced different stress states at failure, with SG1 failing under compression, and SG6 flopping under tension.

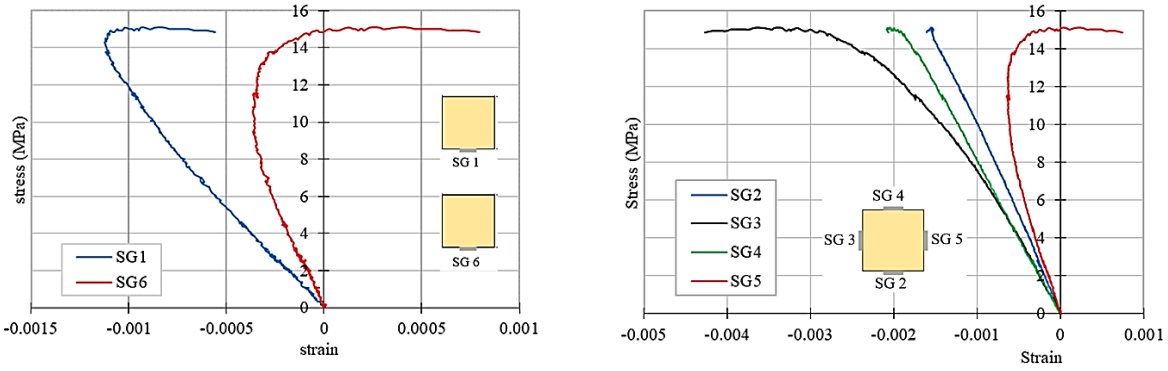

(a) (b)

Figure 7. Stress-strain Response in the (a) Quarter-span and (b) Mid-span

Figure 7(b) showed the axial stress-strain relationship at the mid-span of the specimen. As referenced by Pina et al. [32], the axial stress was calculated using the multiplication of strain measurement by the MoE in bending (E_b= 7742.72 N/mm^2). Meanwhile, the compressive stress was acquired from the load cell measurement. Figure 7(b) showed that both SG2 as well as SG4 signified a linear compressive strength-axial stress relationship with a negative value of stress from the initial condition until failure, and SG3 measurements showed a different behavior. The compressive strength-axial stress relationship developed from the linear (early loading stage) became non-linear, but the stress kept increasing to a negative value. The negative strain value showed that the sides of SG2, SG3, and SG4 were consistently in a state of compression. Consequent with the other SG in mid-span, SG5 possessed the same behavior as the SG1 and SG6. The stress direction reversed drastically just before the failure, and the stress value changed from negative to positive. Additionally, the strain value at failures reached 0.0007, which signified that the stress state in SG5 was tension.

The sudden changes in stress direction before failure was a common factor in buckling members [16]. The phenomenon caused some portions of the cross-section to be in a compression state, as the rest were in tension state (Figure 7(b)). The stress distribution was influenced by shifting of the loading eccentricity as the load was applied. Before loading, the eccentricity between loading axis of the member and longitudinal axis of the specimen was minimized to nearly zero. However, the eccentricity increased rapidly as the specimen deformed laterally during the loading. The eccentricity shift at both ends and mid-span was not measured for equipment safety reasons during the study. Moreover, producing a concentric loading experiment was generally not direct as shown by Pina et al. [32] and Singer et al. [33]. Several factors affected the concentricity including material heterogeneity, test set-up imperfection, residual stresses, and boundary constraints.

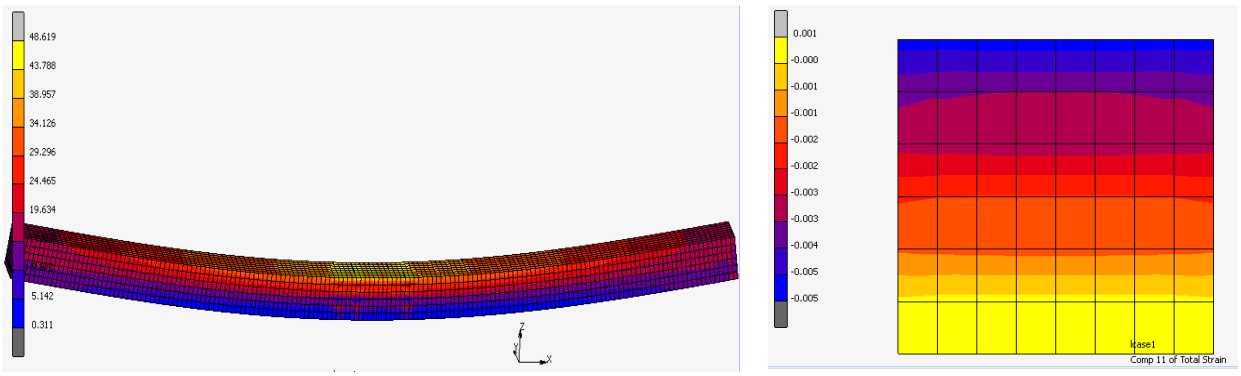

(a) (b)

Figure 8. (a) Longitudinal Stress (σ11) of FEA Model and (b) Strain (ε11) Distribution on the Midspan Cross-section

Figure 8(a) showed the visual deformation and longitudinal stress (σ_{11}) contour of the finite element (FEA) model constructed on MSC Marc/Mentat software. The model deformation was identical to the experiments as the member buckled to one lateral side. Figure 8(b) showed a detailed strain distribution in the mid-span cross-section. FEA results (Figure 8(b)) showed that the model had a compressive strain of about -0.005 and a tensile strain of approximately 0.001. Compared to the experiments, the strain gauge recorded that the member failed when the

compressive strain reached -0.0042 (SG3) while the tensile strain was 0.0007 (SG5). The strain comparison signified a difference between FEA to the experiments of 19% and 43 % for SG3 and SG5, respectively. FEA method produced strain results that were not very close but were still reasonable considering the wood heterogeneity.

FEA on MSC Marc/Mentat used the yield criterion of Hill to determine the failure state of an element. This criterion had an ellipse shape of yield surface, with a minimum value of -1.00 and a maximum value was 1.00. When an element had a failure index value exceeding the range, then the element was declared failed. Figure 9 showed that the failure index of Hill along the member was distributed proportionally with the stress distribution shown in Figure 8(a). Following the discussion, Figure 9 showed that the outermost compressive fiber in the mid-span had a failure index ranging from 0.973 to 1.083, confirming the element had failed at the location. According to the strain and stress produced by FEA model, the model had a compressive fiber failure, which was distinguished using the failure index value of Hill (Figure 9).

Figure 10 showed an axial displacement comparison between FEA results and the experiments. FEA results signified a linear behavior with a maximum axial load of approximately 155.4 kN, 3.2% higher than those of the experiment. After reaching the maximum load, FEA model did not fail directly but continued to develop a softening or flat part in its axial displacement. This flat part of the curve after reaching the maximum load was caused by perfect elastoplastic material assumption developed in FEA. The numerical and experimental stress-strain relationship in the mid-span of the specimen was shown in Figure 7. During the process, the numerical strain was extracted from an element at the same position as the strain gauge arrangement in the experiment. The stress was determined from incremental axial load divided by area cross-section.

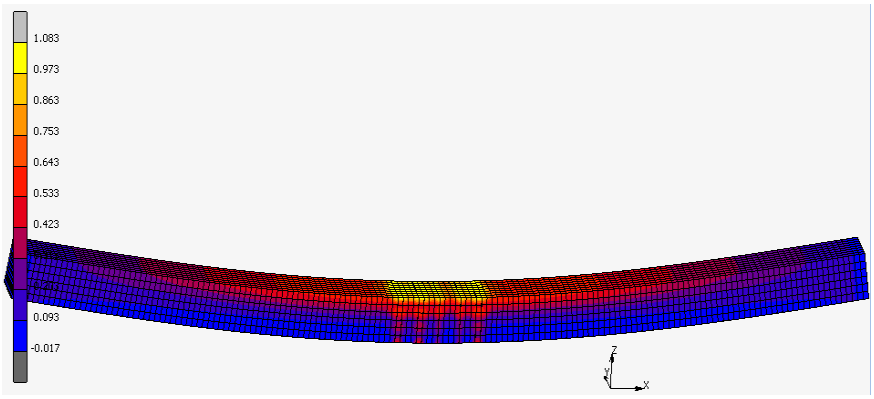

Figure 9. The Failure Index of the FEA Model

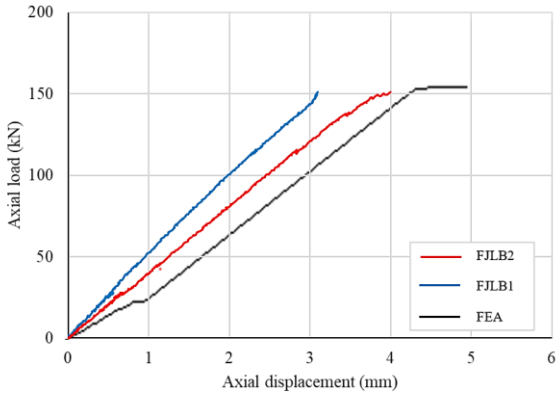

Figure 10. FEA Load-axial Displacement

Figures 11 and 12 showed that FEA model successfully simulated the stress-strain response in SG2 and SG4 sides of the cross-section at the mid-span. Additionally, SG2 and SG4 signified a linear trend in a compression strain direction, with FEA final stress slightly less than the experimental results. The relationship shown in these Figures confirmed that SG2 and SG4 sides failed in the elastic part under a compression stress state.

The numerical and experimental results of SG3 and SG5 (Figure 12) showed a non-linear stress-strain relationship consequent to the linear behavior of SG2 and SG4 (Figures 11). At the early stage of the experiments (under 5.0 MPa), the relationship showed a linear elastic trend and gradually developed a non-linear connection as the loading

continued. However, FEA model in these figures generally showed linear behavior until the final stress was reached. A significant difference in FEA results for SG5 (Figure 12), signified that FEA stress dropped to nearly zero after reaching the final stress, and the strain shifted direction from compression to tension. Moreover, the model developed a secondary strength before failing at the rupture stress of 2.40 MPa.

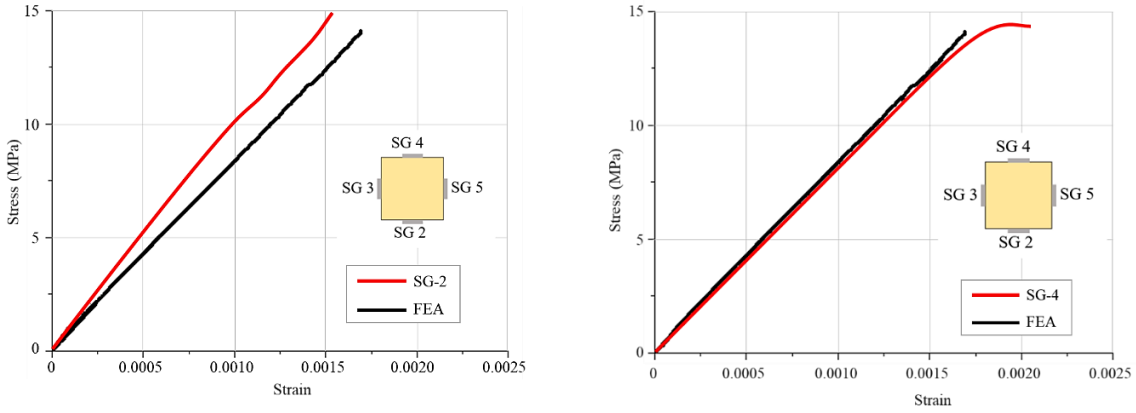

(a) (b)

Figure 11. FEA Stress-strain Relationship of (a) SG-2 and (b) SG-4

Figures 12 showed a significant discrepancy between experimental and numerical analysis results. This discrepancy was caused by the FEA conducted under an ideal assumption that did not consider the presence of finger joints, glue lines, and the shifting of the eccentricity.

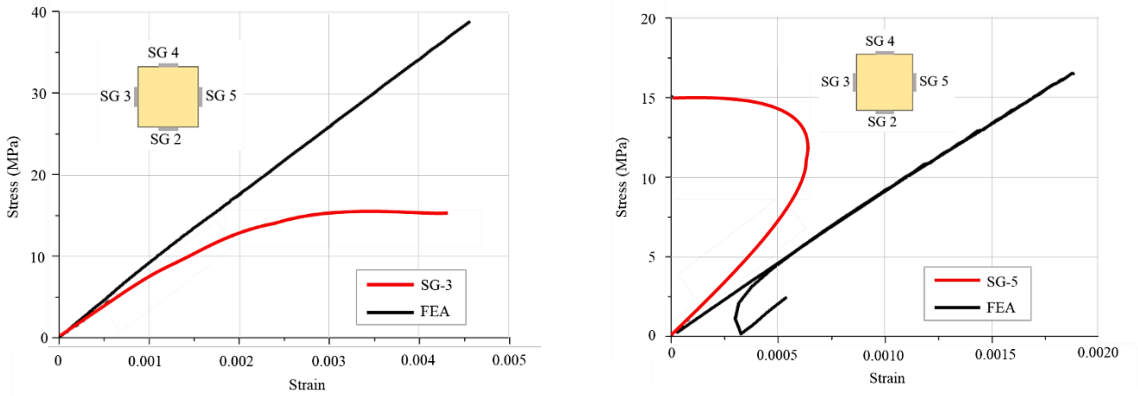

(a) (b)

Figure 12. FEA Stress-strain Relationship of (a) SG-3 and (b) SG-5

During the study, Euler buckling formula (Equation 1) was used to predict the buckling load (P_{cr}) and compared it to the experimental as well as numerical methods. Several parameters applied in the Euler buckling formula were MoE in bending E_b= 7742.72 N/mm^2, as shown in Table 1, where the moment of inertia was I= 8.3 x 10^6 mm^4, length of the member represented L= 2000 mm), and effective length factor was K, which was determined as 1.0 for the pin-pin-ended column. However, this formula did not consider the crookedness of the column, and the load was always axial (zero eccentricity).

$$P_{cr} = \frac{\pi^2 EI}{(KL)^2} \quad (1)$$

Buckling load (P_{cr}) was calculated according to the formula in Equation 1 leading to a buckling load of 159.04 kN. The Experimental and FEA methods produced a buckling load of 150.90 kN and 155.73 kN, respectively. Following the process, the formula of Euler had made a slightly over-estimated buckling load. Compared to the experimental and FEA results, the formula produced a difference of 5.4% and 2.11%, respectively. The formula of Euler provided a fair prediction of buckling load having differences of 5.4%. Concerning the slight differences (< 6%) and the fact that the loading in the formula was always concentric, the experimental set-up successfully kept the eccentricity shifting minimal.

A parametric finding presented in this study used the established FEA and changed both the cross-section and length of FJLB members to produce the same column slenderness ratio with the full-scale tested ratio of 69.28 for practical

use (Figure 13). Compressive members having a length of 2500mm or 3000mm were generally found in a real timber house instead of the member length of 2000 mm. Therefore, in this parametric study, column sections of 125mm x 125mm and a length of 2500mm as well as 150mm x 150mm having a length of 3000mm were evaluated. Figure 13 showed that the cross-section 125 mm x 125 mm column and the cross-section 150 mm x 150 mm contributed buckling load capacity of 235.4 kN and 342.2 kN, respectively.

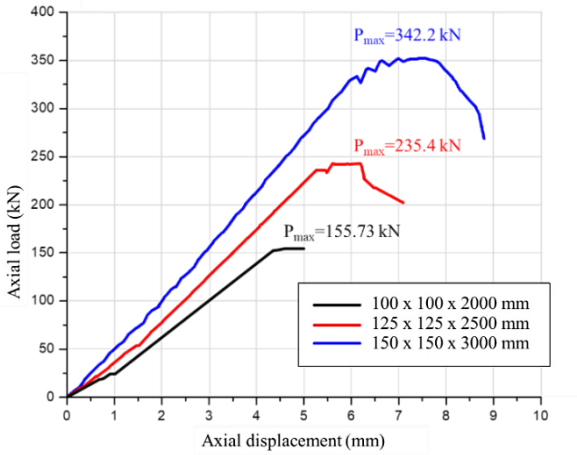

Figure 13. Axial Capacity of Three Compression Members Having the Same Slenderness Ratio

CONCLUSIONS

In conclusion, this study successfully investigated the use of FJLB under uniaxial concentric compression when loaded parallel to the grain. The investigation included laboratory experiments and numerical analysis, specifically focusing on elastoplastic material behaviour as well as buckling analysis. This study found that the experimental and numerical compressive strength for FJLB specimen was 150.90 kN and 155.73 kN, respectively. During the study, there was an average of 3.2 % difference between FEA and the experimental results, which was satisfactory. The compressive strength calculation using the formula of Euler also provided insight into the accuracy of the classical method, which reported a compressive strength of 159.04 kN. Moreover, the results confirmed that the method showed fair agreement with the experiments, with less than a 5.4 % difference. The experiments also signified that the stress state in the mid-span cross-section changed from uniform axial compression to a combination of tension and compression before the failure. This phenomenon occurred due to an eccentricity increase during the loading stage. Although FEA successfully predicted the compressive strength, there was a significant contrast in stress-strain modeling in the mid-span cross-section, which was caused by the limitation of the modeling strategy of the specimens.

REFERENCES

1. Statistics Indonesia, *Percentage of Households with Access to Adequate and Affordable Housing*, 2022. https://www.bps.go.id/indicator/29/1241/1/perse
2. Statistics Indonesia, *Indonesia Population Projection*, 2017.
3. Jakarta Property Institute, *Middle Class Housing Demand Fulfillment Potential Through Co-Residence*, 2023.
4. Purnamasari, L. Effect of Government's Policy to Build 1 Million Houses on Performance of Housing and Apartment Credits of Banks Listed in Indonesia Stock Exchange during Period 2015-2017, *Jurnal Ilmiah Ilmu Administrasi Publik, 11*(1), 2021, pp. 40-50. https://doi.org/10.26858/jiap.v11i1.19777
5. Cabinet Secretariat Indonesia, *The Realisation of the Million Houses Program in 2021 Successfully Reaches 1.11 Million Units*, 2022. https://setkab.go.id/realisasi-program-sejuta-rumah-tahun-2021-capai-111-juta-unit/
6. Hidayah, N., Satyarno, I., and Saputra, A Housing Rehabilitation and Reconstruction in Central Sulawesi Post-2018 Earthquake, *E3S Web Conference, 200*, 2020. https://doi.org/10.1051/e3sconf/202020003004
7. Sutrisno, W., Satyarno, I., Awaludin, A., Saputra, A., and Setiawan, A.F., Seismic Performance of Instant Steel Frame House for Post Earthquake Reconstruction, *Lecture Notes in Civil Engineering, 215*, 2022. https://doi.org/10.1007/978-981-16-7924-7_6
8. Octavia, S., Awaludin, A., and Wusqo, U., Lateral Resistance FJLB Rubberwood Double Shear Connection–Steel Plate with Bolt Connection, *Jurnal Riset Rekayasa Sipil, 6*, 2022, pp. 21–32. https://doi.org/10.20961/jrrs.v6i1.62337
9. Suta, K., Irawanto, E., Rahmawati, H.V., and Widayanti, B.H., The Effectiveness of the Construction of Risha, Rika and Riko (3R) Houses for Earthquake Affected Communities, *Journal Planoearth, 5*, 2020, pp. 20-24. https://doi.org/10.31764/jpe.v5i1.2178

10. Junior, H.J E., Ohto, J.M., Silva, L.L., Palma, H.A.L., and Ballarin, A.W., Potential of Rubberwood (Hevea Brasiliensis) for Structural Use after The Period of Latex Extraction: A Case Study in Brazil. *Journal of Wood Science, 61*, 2015, 384–390. https://doi.org/10.1007/s10086-015-1478-7
11. Junior, H.J.E., Ohto, J. M., Silva, L.L., Palma, H.A.L., and Ballarin, A.W., Potential of Rubberwood (Hevea Brasiliensis) for Structural Use after The Period of Latex Extraction: A Case Study in Brazil, *Journal of Wood Science, 61*, 2015, pp. 384–390. https://doi.org/10.1007/s10086-015-1478-7
12. Shulhan, M.A., Awaludin, A., Nugroho, M.S., and Octavia, S., Flexural Behaviour Study of Finger Jointed Laminated Board (FJLB) Made from Kayu Karet (Hevea Brasiliensis). *Media Komunikasi Teknik Sipil, 28*(2), 2022, pp. 169-177. https://doi.org/10.14710/mkts.v28i2.45714
13. Gustavsson, L., Joelsson, A., and Sathre, R., Life Cycle Primary Energy Use and Carbon Emission of An Eight-Story Wood-Framed Apartment Building, *Journals of Energy and Buidings, 42*, 2010, pp. 230–242. https://doi.org/10.1016/j.enbuild.2009.08.018
14. Guardigli, L., Monari, F., and Bragadin, M.A., Assessing Environmental Impact of Green Buildings through LCA Methods: A Comparison between Reinforced Concrete and Wood Structures in the European Context, *Procedia Engineering*, *21*, 2011, pp. 1199–1206. https://doi.org/10.1016/j.proeng.2011.11.2131
15. Nugroho, N. and Bahtiar, T.E., Buckling Formulas for Designing A Column with Gigantochloa Apus, *Case Study of Construction and Material, 14*, 2021, 00516. https://doi.org/10.1016/j.cscm.2021.e00516
16. Li, H.T., Su, J.W., Zhang, Q.S., Deeks, A.J., and Hui, D., Mechanical Performance of Laminated Bamboo Column under Axial Compression, *Composite Part B: Engineering, 79*, 2015, pp. 374–382. https://doi.org/10.1016/j.compositesb.2015.04.027
17. Zhou, S.C., Chu, F.Z., Lu, X.H., and Xiao, Y., Experimental Studies on Glubam Columns under Axial Compression, *Journal of Building Engineering, 49*, 2022. https://doi.org/10.1016/j.jobe.2021.103453
18. Awaludin, A., Rachmawati, K., Aryati, M., and Danastri, A.D., Development of Cold Formed Steel - Timber Composite for Roof Structures: Compression Members*, Procedia Engineering, 125*, 2015, pp. 850–856. https://doi.org/10.1016/j.proeng.2015.11.052
19. Bahtiar, E.T., Malkowska. D., Trujillo, D., and Nugroho, N., Experimental Study on Buckling Resistance of Guadua Angustifolia Bamboo Column, *Engineering Structure, 228*, 2021, p. 111548. https://doi.org/10.1016/j.engstruct.2020.111548
20. Anshari, B., Guan, Z.W., and Wang, Q.Y., Modelling of Glulam Beams Pre-stressed by Compressed Wood, *Composite Structure, 165*, 2017, pp. 160–170. https://doi.org/10.1016/j.compstruct.2017.01.028
21. Sandhaas, C. and Kuilen, J.W.G., Material Model for Wood, *Heron, 53*, 2013, pp. 179–200
22. Fueyo, J.G., Cabezas, J.A., Domínguez, M, Anton, N., and Villarino., A., Energy Distribution in Dowel-Type Joints in Timber Structures When Using Expansive Kits. *Forests, 12*(9), 2021, pp. 1–21. https://doi.org/10.3390/f12091200
23. Buchanan, A.H., Bending Strength of Lumber, *Journal of Structural Engineering, 116*, 1999, pp. 1213–1229. https://doi.org/10.1061/(ASCE)0733-9445(1990)116:5(1213)
24. Awaludin, A., Irawati, I.S., and Shulhan, M.A., Two-dimensional Finite Element Analysis of The Flexural Resistance of LVL Sengon Non-Prismatic Beams, *Case Study of Construction and Material, 10*, 2019. https://doi.org/10.1016/j.cscm.2019.e00225
25. Effendi, M.K. and Awaludin, A., Nonlinear Finite Element Analysis of Flexural Laminated Veneer Lumber (LVL) Sengon Slender Beam, *Civil Engineering Dimension, 24*(2), 2022, pp. 85-92. https://doi.org/10.9744/CED.24.2.85-92
26. Shakimon, M.N., Malek, N.J.A., Hassan, R., and Ahmad, Z., The Finite Element Modelling of Glulam Tropical Timber Beam in Bending, *Jurnal Teknologi, 78*, 2016. https://doi.org/10.11113/jt.v78.8579
27. Serrano, E. and Larsen, H.J., Numerical Investigations of the Laminating Effect in Laminated Beams, *Journal of Structural Engineering, 125*, 1999, pp. 740–745. https://doi.org/10.1061/(ASCE)0733-9445(1999)125:7(740)
28. Nali P.C. and Carrerra, E., A Numerical Assessment on Two-Dimensional Failure Criteria for Composite Layered Structures, *Composite Engineering, 43*, 2012, pp. 280–289. https://doi.org/10.1016/j.compositesb.2011.06.018
29. Zienkiewicz, O.C. and Taylor, R.L., *The Finite Element Method for Solid and Structural Mechanics*, Elsevier Butterworth-Heinemann, 2005.
30. ADINA R&D Inc., *Theory and Modelling Guide Volume I*, Report ARD 12-8, Watertown, 2012.
31. Zhang, J., He, M., and Li, Z., Compressive Behavior of Glulam Columns with Initial Cracks under Eccentric Loads, *Journal of Advance Structural Engineering, 10*, 2018, pp. 111–119. https://doi.org/10.1007/s40091-018-0181-5
32. Pina, J.C., Flores, E.I.S., and Saavedra, K., Numerical Study on The Elastic Buckling of Cross-Laminated Timber Walls Subject to Compression, *Construction and Building Materials, 199*, 2018, pp. 82–91. https://doi.org/10.1016/j.conbuildmat.2018.12.013
33. Singer, J., Arbocz, J., and Weller, *Buckling Experiments: Experimental Methods in Buckling of Thin-walled Structures*, John Wiley and Sons, 2002.